Simulations of vortex-dominated flows: adaptive vorticity confinement vs. rotational-form upwinding

By S. Hahn AND G. Iaccarino

1. Motivation and objectives

Accurate prediction of highly vortical flows in a transonic environment has been a long-standing dilemma in computational fluid dynamics because the artificial dissipation required inevitably for shock capturing significantly affects the evolution of vortices. Typical examples include shock–turbulence interactions (Lee *et al.* 1993) and helicopter rotor flows (Strawn 2000). Even though this predicament is most commonly found in compressible-flow simulations, many incompressible CFD codes based on upwind discretizations for stability and robustness at high Reynolds numbers are also confronted with the same problem. For a general discussion on the difficulty in vortical-flow simulations, refer to Roe (2001).

As a remedy, Steinhoff and colleagues (Steinhoff *et al.* 1992; Steinhoff & Underhill 1994; Steinhoff & Lynn 2004; Steinhoff *et al.* 2005) proposed the concept of vorticity confinement, where a specially designed momentum forcing is added to the standard Euler/Navier–Stokes equations to prevent a vortex from being inordinately diffused. The forcing includes a user-defined coefficient (typically denoted by ϵ) that controls its strength. Even though the vorticity confinement showed successful and promising results for diverse problems in aerodynamics (Wang *et al.* 1995; Hu *et al.* 2000; Moulton & Steinhoff 2000; Wenren *et al.* 2006), it is questionable to assume a constant value of the proportionality coefficient in front of the confinement terms over the entire flow field (Murayama *et al.* 2001). In order to make ϵ dependent on flow and computational parameters, several studies attempted different ideas: Fedkiw *et al.* (2001) introduced the mesh size h to guarantee the computational consistency with mesh refinement. Löhner & Yang (2002) and Löhner *et al.* (2002) devised a formulation where a proper length scale h is computed by considering the gradient of vorticity magnitude and the confinement term is proportional to h^2. On the other hand, Robinson (2004) suggested a formulation where the confinement term is proportional to helicity. Recently, Butsuntorn & Jameson (2008) devised a formulation where the confinement term is proportional to the logarithm of cell-volume ratio and helicity magnitude in their rotor-blade simulation using the time-spectral method.

Even though the studies listed above introduced an improved dependency of confinement terms on flow and mesh properties, they did not completely eliminate a proportionality constant. Unfortunately, an *a priori* determination of this proportionality constant is quite arbitrary. In order to gain confidence in the applicability of vorticity confinement, it would be ideal to completely eliminate such an arbitrariness and dynamically compute the strength of confinement terms in an adaptive manner. In this article, we suggest two procedures for an improved prediction of vortical fields in the presence of numerical dissipation: One is the adaptive vorticity confinement, where the strength of the confinement

term is computed without any need for an arbitrary constant. The other is the upwind scheme based on the rotational form of convection terms. The basic concept of vorticity confinement is introduced in Sec. 2, formulations for the two newly proposed methods are presented in Secs. 3 and 4, followed by results and discussion in Sec. 5.

2. Interpretation of the vortex confinement approach

As in Steinhoff & Underhill (1994), we focus our mathematical derivation on incompressible flow for simplicity. The Navier–Stokes equations including the vorticity confinement in incompressible fluid are:

$$\frac{\partial u_i}{\partial x_i} = 0, \tag{2.1}$$

$$\frac{\partial u_i}{\partial t} + u_j \frac{\partial u_i}{\partial x_j} = -\frac{1}{\rho}\frac{\partial p}{\partial x_i} + \nu \frac{\partial^2 u_i}{\partial x_j \partial x_j} + \nu_n \frac{\partial^2 u_i}{\partial x_j \partial x_j} - e_{ijk}\epsilon n_j \omega_k, \tag{2.2}$$

where u_i are the velocity components, p the pressure, ρ the density, ν and ν_n the kinematic (physical) and the numerical (artificial) viscosity, respectively, e_{ijk} the permutation symbol, and ω_k the k-th component of the vorticity vector $\boldsymbol{\omega}$. The last term $-e_{ijk}\epsilon n_j \omega_k$ is the vorticity-confinement forcing term, where n_j is the j-th component of a unit vector $\mathbf{n} \equiv \nabla\eta/|\nabla\eta|$ with $\eta \equiv -|\boldsymbol{\omega}|$ and ϵ is the confinement constant which controls the strength of the confinement term, or, in other words, the region over which this forcing term is active. The role of the confinement term is best understood by considering an axisymmetric vortex tube, where $\mathbf{n}$ points outward from the vortex center and hence the main purpose of the confinement term is to convect $\boldsymbol{\omega}$ back toward the vortex center as it diffuses outward. Also note that the numerical viscosity is for the time being assumed to be explicitly known *a priori* for convenience. Even though Eq. (2.2) is not in a conservative form, it has been widely used (Steinhoff *et al.* 1992; Steinhoff & Underhill 1994) due to its simplicity. The confinement term is expressed as a cross product with the vorticity vector, and thus it naturally suggests that relations between numerical viscosity and confinement forcing are best described in the rotational form. Eq. (2.2) can be rewritten in rotational form as follows:

$$\frac{\partial u_i}{\partial t} = -\frac{\partial}{\partial x_i}\left(\frac{p}{\rho} + \frac{1}{2}u_j u_j\right) + \nu \frac{\partial^2 u_i}{\partial x_j \partial x_j} + \nu_n \frac{\partial^2 u_i}{\partial x_j \partial x_j} + e_{ijk}\left(u_j - \epsilon n_j\right)\omega_k. \tag{2.3}$$

Applying the curl operator to Eq. (2.3) leads to the following vorticity equations:

$$\begin{aligned}\frac{\partial \omega_i}{\partial t} &= \nu \frac{\partial^2 \omega_i}{\partial x_j \partial x_j} + \nu_n \frac{\partial^2 \omega_i}{\partial x_j \partial x_j} + \frac{\partial}{\partial x_j}\left(u_i - \epsilon n_i\right)\omega_j - \frac{\partial}{\partial x_j}\left(u_j - \epsilon n_j\right)\omega_i \\ &= \nu \frac{\partial^2 \omega_i}{\partial x_j \partial x_j} + \nu_n \frac{\partial}{\partial x_j}\left(\frac{\partial \omega_i}{\partial x_j} - \frac{\partial \omega_j}{\partial x_i}\right) + \frac{\partial}{\partial x_j}\left(u_i - \epsilon n_i\right)\omega_j - \frac{\partial}{\partial x_j}\left(u_j - \epsilon n_j\right)\omega_i,\end{aligned} \tag{2.4}$$

where the solenoidality of a vorticity field, $\partial\omega_j/\partial x_j = 0$, is used to make both sides skew-symmetric and thus consistent in Eq. (3.1) below. The third and fourth terms on the right-hand side account for stretching/tilting and convection flux, respectively. It is clearly shown in Eq. (2.4) that the mechanism of vorticity confinement is to counteract the numerical diffusion by artificially generating stretching/tilting and convection flux. In general three-dimensional flows, the counterbalance between the two artifacts can arise in a very complicated way, but there is further simplification in two-dimensional flows. For example, in an axisymmetric vortex tube mentioned above, there is no stretch-

ing/tilting and hence the anti-diffusion is wholly contributed by the artificial convection flux $\partial(-\epsilon n_j\omega_i)/\partial x_j$, where the convection velocity $-\epsilon n_j$ directs toward the vortex center and hence impedes the artificial diffusion.

3. Adaptive vorticity confinement

Our ultimate goal here is to minimize the influence of ν_n on the vorticity field. Therefore, it is most desirable if ϵ satisfies the following relation

$$\epsilon(n_i\omega_j - n_j\omega_i) = \nu_n\left(\frac{\partial\omega_i}{\partial x_j} - \frac{\partial\omega_j}{\partial x_i}\right), \tag{3.1}$$

which is a tensor identity and hence ϵ is overspecified. As is used in the standard dynamic LES procedure (Lilly 1992), the least square error between both sides would lead to a good estimation for ϵ and yields the following expression:

$$\epsilon = \frac{\nu_n(\partial\omega_i/\partial x_j - \partial\omega_j/\partial x_i)(n_i\omega_j - n_j\omega_i)}{(n_i\omega_j - n_j\omega_i)(n_i\omega_j - n_j\omega_i)}, \tag{3.2}$$

where the summation convention is implied only over $(i,j) = (1,2)$, $(2,3)$, and $(3,1)$ since both sides in Eq. (3.1) are skew-symmetric. The arbitrariness in the definition of ϵ is completely eliminated in Eq. (3.2) by computing it as a function of vorticity field in an adaptive manner. Note that ϵ in Eq. (3.2) is proportional to ν_n. Since numerical viscosities are, in general, in the order of $\mathcal{O}(\Delta x^n)$, ϵ is also in the same order and therefore this approach guarantees the consistency, i.e. the solution asymptotically approaches the exact one with resolution refinement.

In the above derivation, the numerical viscosity ν_n is assumed to be known *a priori*, which is not to be common in practical situations and hence the artificial diffusion terms should be estimated. We estimate them by considering the difference between central and upwind discretizations of convection terms in the given flow field, viz.

$$\nu_n\frac{\partial^2 u_i}{\partial x_j\partial x_j} \equiv D_i \approx \frac{\delta^{\mathrm{CD}}}{\delta x_j}u_iu_j - \frac{\delta^{\mathrm{UD}}}{\delta x_j}u_iu_j, \tag{3.3}$$

where the superscripts CD and UD denote central and upwind differences, respectively. With the estimated D_i on right-hand sides of the Navier–Stokes equations, the vorticity equations become

$$\frac{\partial\omega_i}{\partial t} = \nu\frac{\partial^2\omega_i}{\partial x_j\partial x_j} + \frac{\partial}{\partial x_j}e_{ijk}D_k + \frac{\partial}{\partial x_j}\left(u_i - \epsilon n_i\right)\omega_j - \frac{\partial}{\partial x_j}\left(u_j - \epsilon n_j\right)\omega_i, \tag{3.4}$$

and hence the counterparts for Eqs. (3.1) and (3.2) become

$$\epsilon(n_i\omega_j - n_j\omega_i) = e_{ijk}D_k, \tag{3.5}$$

$$\begin{aligned}\epsilon &= \frac{e_{ijk}D_k(n_i\omega_j - n_j\omega_i)}{(n_i\omega_j - n_j\omega_i)(n_i\omega_j - n_j\omega_i)}\\ &= \frac{D_3(n_1\omega_2 - n_2\omega_1) + D_1(n_2\omega_3 - n_3\omega_2) + D_2(n_3\omega_1 - n_1\omega_3)}{(n_1\omega_2 - n_2\omega_1)^2 + (n_2\omega_3 - n_3\omega_2)^2 + (n_3\omega_1 - n_1\omega_3)^2}.\end{aligned} \tag{3.6}$$

4. Upwind scheme based on the rotational form

As is shown in the previous section, the formulation of adaptive vorticity confinement requires an explicit estimation of numerical diffusion, and we use the difference between central and upwind discretizations of convection terms in order to evaluate it. One of the concerns in this procedure is the possibility that the confinement terms exactly counteract the numerical diffusion, in which case the combination of vorticity confinement and an upwind scheme is simply reduced to typical central differencing and the overall computation can be numerically unstable. Since the objective of vorticity confinement is to enhance the prediction of vortical flow fields while maintaining the required effect of numerical diffusion especially in transonic flows, it is desirable to devise a scheme which does not depend on any explicit estimation. As stated in the previous section, the influence of vorticity confinement is best described in the rotational form, and hence we first investigate how to combine an upwind discretization with the rotational form.

The rotational form has been often used and studied in combination with the spectral method, but its use has been usually limited in finite-difference or finite-volume methods because it is inherently non-conservative and can potentially introduce large non-physical errors (Horiuti 1987). For example, Zang (1991) showed from spectral simulations that the rotational form is especially sensitive to the dealiasing process and becomes very unstable without it, whereas the skew-symmetric form is fairly robust even without dealiasing. On the other hand, Horiuti & Itami (1998) showed that, despite its dispersive error characteristics, central differencing can actually result in a decay of turbulence in wall-bounded flows because the leading-error terms act like the Coriolis force when the rotational form is combined with a finite-difference scheme. In spite of these informative studies, combination of an upwind scheme with the rotational form has been quite rare so far. Indeed, it is not straightforward to compose an upwind scheme in the rotational form because it is not based on advective kinematics. However, the following identity

$$u_j \frac{\partial u_i}{\partial x_j} = u_j \left[\frac{\partial u_j}{\partial x_i} + \left(\frac{\partial u_i}{\partial x_j} - \frac{\partial u_j}{\partial x_i} \right) \right] = \frac{\partial}{\partial x_i} \left(\frac{1}{2} u_j u_j \right) + 2\Omega_{ij} u_j, \tag{4.1}$$

naturally suggests that one of the two u_j's in the kinetic energy originates from the advection velocity. Assuming the second-order central and first-order upwind differences in the Cartesian coordinate system as our base schemes, we suggest the following as an upwind scheme for the rotational form:

$$\begin{aligned} \left[\frac{\partial}{\partial x_1} \left(\frac{1}{2} u_j u_j \right) + 2\Omega_{1j} u_j \right] \approx{}& \frac{1}{2} \frac{\delta^{\mathrm{CD2}}}{\delta x_i} u_j u_j + 2\Omega_{ij}^{\mathrm{CD2}} u_j \\ &+ \frac{1}{2} \left(\frac{\delta^{\mathrm{UD1}}}{\delta x_1} u_1 u_1 - \frac{\delta^{\mathrm{CD2}}}{\delta x_1} u_1 u_1 \right) \delta_{i1} \\ &+ \frac{1}{2} \left(\frac{\delta^{\mathrm{UD1}}}{\delta x_2} u_2 u_2 - \frac{\delta^{\mathrm{CD2}}}{\delta x_2} u_2 u_2 \right) \delta_{i2} \\ &+ \frac{1}{2} \left(\frac{\delta^{\mathrm{UD1}}}{\delta x_3} u_3 u_3 - \frac{\delta^{\mathrm{CD2}}}{\delta x_3} u_3 u_3 \right) \delta_{i3}, \end{aligned} \tag{4.2}$$

where the superscripts CD2 and UD1 denote that the relevant derivatives are computed from the second-order central and first-order upwind differences, respectively. Note that upwinding is applied only to the kinetic-energy component in the gradient direction, and all the other derivative terms, including Ω_{ij}, are evaluated via central differencing. Because upwinding is retained only in the kinetic-energy gradient which does not directly

contribute to the vorticity evolution, it is expected that Eq. (4.2) would result in an improved protection of the vortical field from the influence of numerical diffusion.

5. Results and discussion

In this section, the performances of suggested methods are evaluated for the three basic test problems: traveling Taylor vortex, collision of two vortex rings, and vortex rebound from a wall. The incompressible Navier–Stokes solver used is based on the Cartesian coordinate system and the staggered velocity configuration. The time integration is based on the semi-implicit fractional-step method with the Runge–Kutta and Crank–Nicolson methods for convective and viscous terms, respectively, whereas the second-order central difference is used as base spatial discretization. The no-slip boundary condition is imposed at walls and periodic boundary conditions are applied for all the free boundaries. This code directly solves the Poisson equation for the pseudo-pressure using the discrete Fourier transform and tridiagonal matrix solver in periodic and wall-normal directions, respectively (Hahn *et al.* 2002). Note that the second-order central difference as base spatial discretization is stable for all the test problems considered, and hence allows for a comprehensive comparison.

5.1. *Traveling Taylor vortex*

The analytic solution for the traveling Taylor vortex is given in non-dimensional form as

$$u = \frac{-(y-y_c)}{1+2t/\mathrm{Re}} \exp\left[\frac{1}{2}\left(1 - \frac{(x-x_c)^2+(y-y_c)^2}{1+2t/\mathrm{Re}}\right)\right] + U, \tag{5.1}$$

$$v = \frac{x-x_c}{1+2t/\mathrm{Re}} \exp\left[\frac{1}{2}\left(1 - \frac{(x-x_c)^2+(y-y_c)^2}{1+2t/\mathrm{Re}}\right)\right], \tag{5.2}$$

where (x, y) and (u, v) denote the Cartesian coordinates and corresponding velocity vectors, respectively, t the time, Re the Reynols number, U the constant traveling speed, and (x_c, y_c) the vortex-center coordinates. All the variables are non-dimensionalized by the initial maximum azimuthal velocity $u_{\theta 0}$ and initial vortex radius r_0 (where the azimuthal velocity at $t = 0$ is maximum). The Reynolds number is set to $\mathrm{Re} \equiv u_{\theta 0} r_0/\nu = 100$ and the constant travel speed of $U = 8$ is given. The size of the computational domain is $0 \le x \le 16$ and $-8 \le y \le 8$, where 256×256 uniform meshes are used. The vortex is initially located at the center of the computational domain.

Fig. 1 shows the vertical-velocity profile along the horizontal vortex centreline and contours of the spanwise vorticity at $t = 2.36$. As is expected, the numerical viscosity of $\nu_n = 10\nu$ strongly diffuses the vortex (Fig. 1*a* and *d*). On the other hand, even in the presence of the same extent of numerical viscosity, the adaptive vorticity confinement using Eq. (3.2) perfectly reproduces the analytic solution (Fig. 1*a* and *e*). In addition, the rotational-form-based upwind scheme using Eq. (4.2) preserves the vortical field far better than the standard first-order upwind scheme (Fig. 1*b*, *f*, and *g*). What is especially promising is that the width of the vortex is very well captured in spite of underprediction of the vortex strength.

5.2. *Collision of two vortex rings*

In order to examine the performance of proposed methods for more complicated three-dimensional vortex interactions, they are applied to a collision of two vortex rings in free space (Kida *et al.* 1991). This problem was also used to test the original formulation of

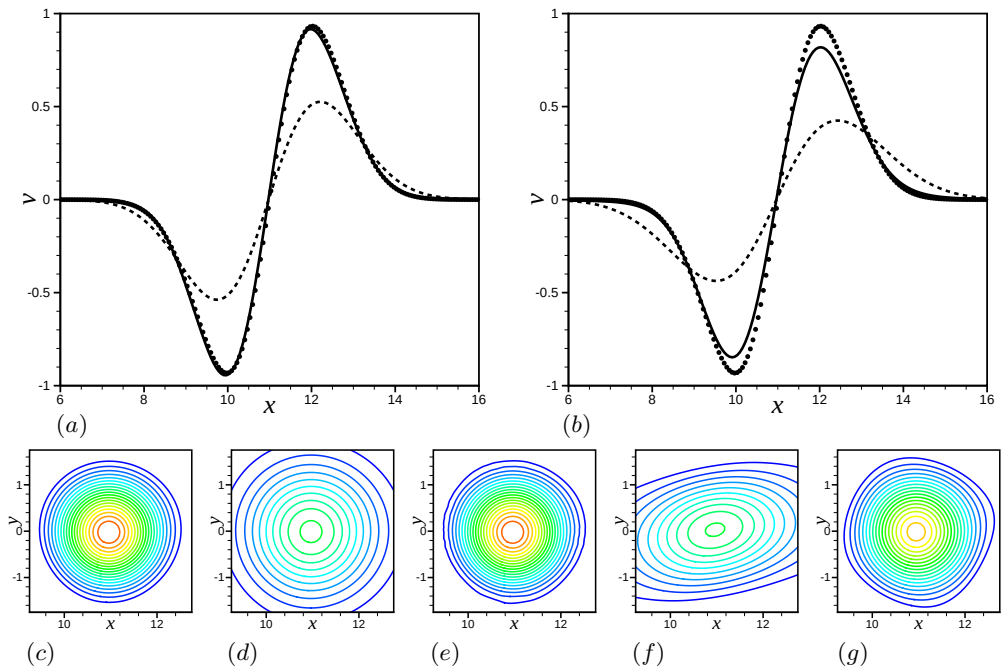

FIGURE 1. Traveling Taylor vortex at $t = 2.36$: (a–b) vertical-velocity profile along the horizontal vortex centreline: •, analytic solution; (a) ———, $\nu_n = 10\nu$ with confinement; - - - -, $\nu_n = 10\nu$ without confinement; (b) ———, rotational-form-based first-order upwind; - - - -, standard first-order upwind: (c–g) contours of the spanwise vorticity: (c) analytic solution; (d) $\nu_n = 10\nu$ without confinement; (e) $\nu_n = 10\nu$ with confinement; (f) standard first-order upwind; (g) rotational-form-based first-order upwind.

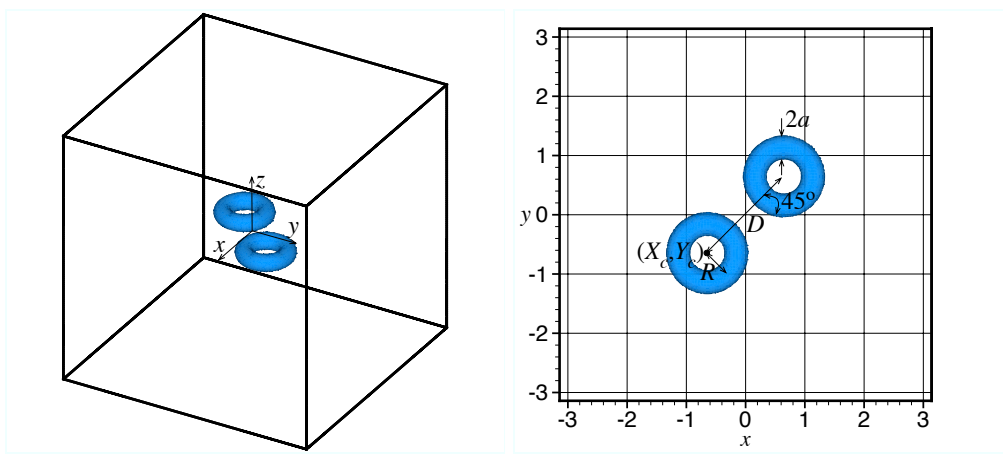

FIGURE 2. Initial configuration for a pair of ring vortices.

vorticity confinement by Steinhoff & Underhill (1994). The flow is initialized by the two identical ring vortices with Gaussian azimuthal vorticity in the cross section:

$$\omega(x, y, z) = \omega_0 \exp\left[-\left(\frac{r}{a}\right)^2\right], \tag{5.3}$$

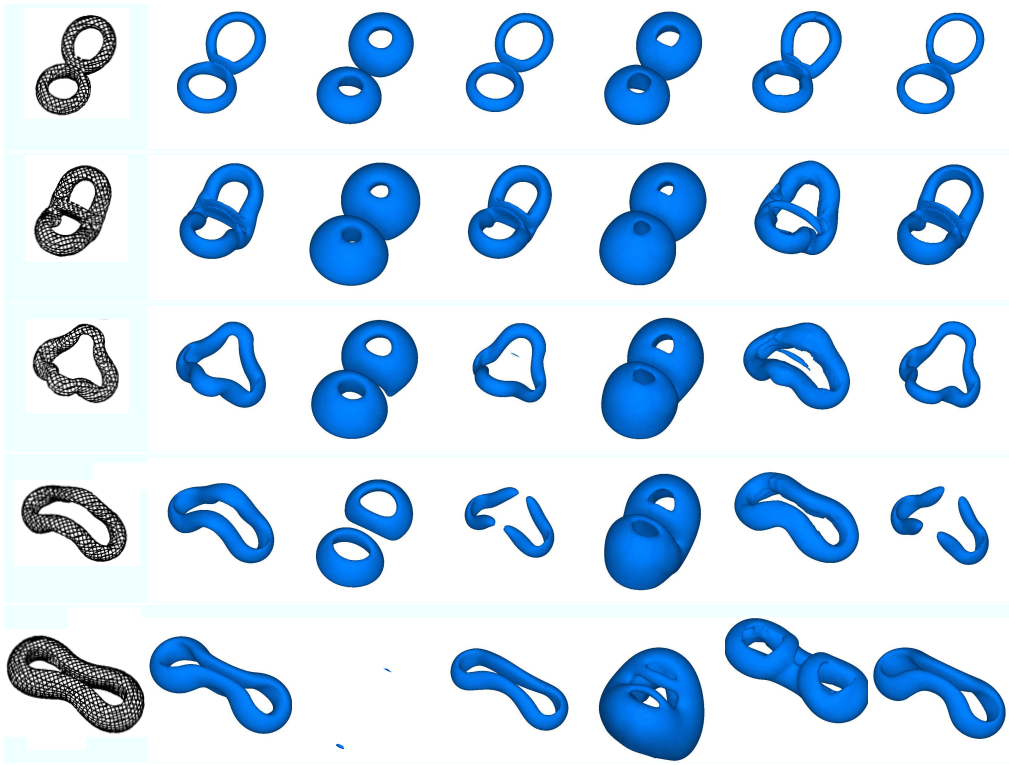

(*a*) (*b*) (*c*) (*d*) (*e*) (*f*) (*g*)

FIGURE 3. Iso-surfaces of the vorticity magnitude: (*a*) Kida *et al.* (1991); (*b*) reference solution (central difference with $\nu_n = 0$); (*c*) $\nu_n = 2\nu$ without confinement; (*d*) $\nu_n = 2\nu$ with confinement; (*e*) standard first-order upwind; (*f*) standard first-order upwind with confinement based on estimated numerical diffusion with Eqs. (3.3)–(3.6); (*g*) rotational-form-based upwind. $t = 3$, 4.5, 6, 7.5, and 12 from top to bottom.

where $r = [(x - x_c)^2 + (y - y_c)^2 + z^2]^{\frac{1}{2}}$, $x_c = X_c + R\cos\theta$, $y_c = Y_c + R\sin\theta$, $\theta = \tan^{-1}\left(\frac{y-Y_c}{x-X_c}\right)$, $(X_c, Y_c) = (\pm\frac{1}{2}D\cos 45°, \pm\frac{1}{2}D\sin 45°)$, D is the distance between the centers of two ring vortices, R and a the radius and thickness (where $\omega = \mathrm{e}^{-1}\omega_0$) of ring vortices, respectively, and ω_0 the value of azimuthal vorticity at $r = 0$ (Fig. 2). The dimensions of ring vortices are $D = 1.83$, $R = 0.491$, $a = 0.196$, and $\omega_0 = 23.8$ (denoted by 'Case II' in Kida *et al.* 1991). This problem is solved on 128^3 uniform meshes in the periodic box with the size of $(2\pi)^3$. The circulation-based Reynolds number of ring vortices is set to be $\mathrm{Re}_\Gamma = \Gamma/\nu = \pi\omega_0 a^2/\nu = 577$.

Fig. 3 shows the temporal evolution of two ring vortices. The reference solution (i.e. central difference with $\nu_n = 0$; Fig. 3*b*) exhibits the evolution of vortices very close to that from the spectral simulation by Kida *et al.* (1991) (Fig. 3*a*). As is expected, both the numerical viscosity of $\nu_n = 2\nu$ (Fig. 3*c*) and standard first-order upwind scheme (Fig. 3*e*) result in an excessive diffusion and hence show completely erroneous flow developments. Note that a smaller value of $\nu_n = 2\nu$ is used here as compared to the previous case as the final configuration ($t = 12$) shows completely dissociated vortex rings. On the other hand, both the adaptive vorticity confinement and rotational-form-based upwind scheme reproduce very closely the correct qualitative features of the reference solution in the

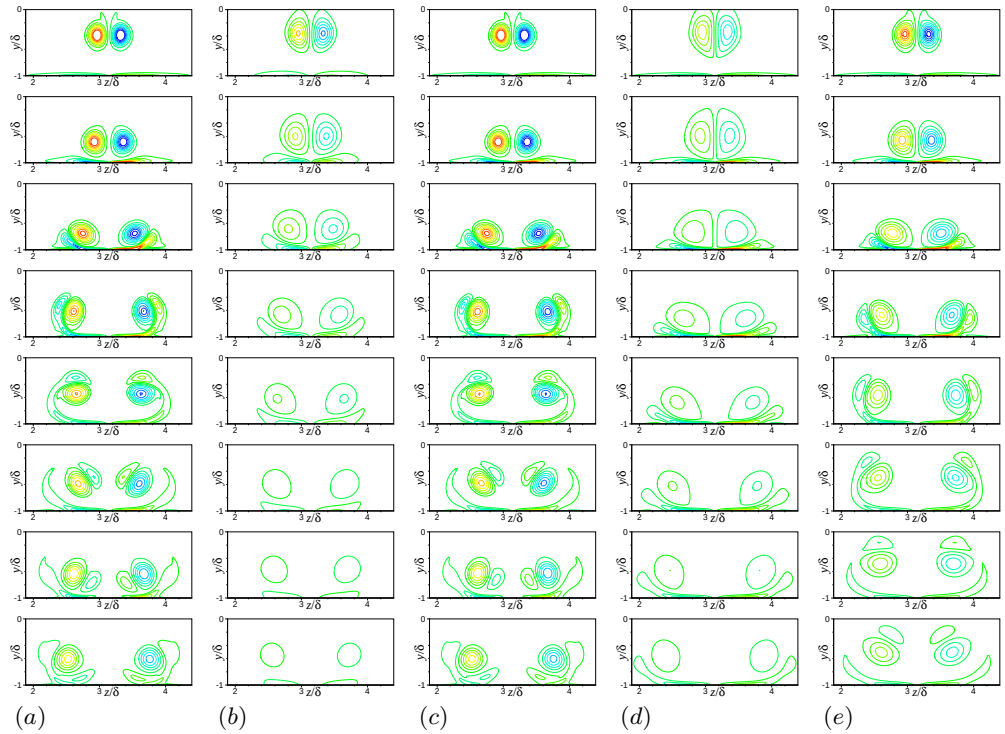

FIGURE 4. Contours of the streamwise vorticity (ω_x): (a) reference solution (central difference with $\nu_n = 0$); (b) $\nu_n = 5\nu$ without confinement; (c) $\nu_n = 5\nu$ with confinement; (d) standard first-order upwind; (e) rotational-form-based first-order upwind: $t\Gamma/\delta^2 = 1, 2, \ldots, 8$ from top to bottom.

presence of artificial diffusion. A slight deterioration of solution quality is observed when the adaptive vorticity confinement is combined with the estimation of numerical diffusion using Eqs. (3.3)–(3.6) (Fig. 3f), whereas the rotational-form-based upwind scheme shows excellent performance (Fig. 3g).

5.3. *Rebound of a counter-rotating vortex pair from a wall*

As a preliminary step to examine the performance of the proposed adaptive procedures for complex interactions of vortices with a solid wall (involving the generation of and interactions with secondary vortices), a two-dimensional counter-rotating vortex pair over a wall (Orlandi 1990; Choi *et al.* 1994; Lim *et al.* 1998) is considered in this section. The initial flow field is composed of a vortex dipole in a channel with a Gaussian vorticity distribution:

$$\omega_x(y,z) = \pm\frac{\Gamma}{\pi\sigma^2}\exp\left[-\frac{(y-y_c)^2+(z\pm z_c)^2}{\sigma^2}\right], \tag{5.4}$$

where x, y, and z denote streamwise, wall-normal, and spanwise coordinates of the channel, respectively, σ the vortex radius, $(y_c, \pm z_c)$ the vortex-center coordinates, and Γ the circulation of the vortex ($\Gamma = \int \omega_x \mathrm{d}y\mathrm{d}z$). The Reynolds number is set to $\mathrm{Re} \equiv \Gamma/\nu = 1800$, and the vortex dipole with $\sigma = \frac{1}{9}\delta$ is initially located at $(y_c, \pm z_c) = (0, \pm\frac{1}{6}\delta)$, where δ is the channel half width. The size of the computational domain is $-\delta \le y \le \delta$ and $0 \le z \le 2\pi\delta$, where 129 non-uniform and 256 uniform mesh points are used in the y and z directions, respectively.

Fig. 4 shows the temporal evolution of the vorticity field. The reference solution (Fig. 4*a*) shows that two vortices initially descend toward the lower wall due to the induced motion. Once they arrive very close to the wall, strong vorticity of opposite sign is generated due to the no-slip condition. This wall vorticity induces two vortices to move apart from each other and eventually creates secondary vortices, which revolve around the corresponding primary ones. Both the explicit numerical viscosity of $\nu_n = 5\nu$ (Fig. 4*b*) and standard upwind scheme (Fig. 4*d*) weaken the primary vortices very quickly and cannot accurately predict the later evolution of secondary vortices. On the other hand, the solution with the adaptive vorticity confinement (Fig. 4*c*) almost exactly reproduces the correct flow evolution. Meanwhile, the rotational-form-based upwind scheme shows an improved prediction over standard upwinding especially during the early stage. Nevertheless, the vortices are continuously diffused and a qualitative discrepancy becomes increasingly prominent in the later development of secondary vortices, because in this two-dimensional test problem the flow is mainly driven by the strength of vorticity. It is worth noting that even at $t = 1$ the vortex strength is already reduced with the rotational-form unwind scheme (as opposed to the vortex confinement) while its shape and size are retained much longer.

REFERENCES

Butsuntorn, N. & Jameson, A. 2008 Time spectral method for rotorcraft flow. *AIAA Paper* 2008–0403.

Choi, H., Moin, P. & Kim, J. 1994 Active turbulence control for drag reduction in wall-bounded flows. *J. Fluid Mech.* **262**, 75–110.

Fedkiw, R., Stam, J. & Jensen, H. W. 2001 Visual simulation of smoke. *Proc. Twenty-Eighth Annual Conference on Computer Graphics and Interactive Techniques*, Los Angeles, August 12–17, pp. 15–22.

Hahn, S., Je, J. & Choi, H. 2002 Direct numerical simulation of turbulent channel flow with permeable walls. *J. Fluid Mech.* **450**, 259–285.

Horiuti, K. 1987 Comparison of conservative and rotational forms in large eddy simulation of turbulent channel flow. *J. Comput. Phys.* **71**, 343–370.

Horiuti, K. & Itami, T. 1998 Truncation error analysis of the rotational form for the convective terms in the Navier-Stokes equation. *J. Comput. Phys.* **145**, 671–692.

Hu, G., Grossman, B. & Steinhoff, J. 2000 A numerical method for vortex confinement in compressible flow. *AIAA Paper* 2000–0281.

Kida, S., Takaoka, M. & Hussain, F. 1991 Collision of two vortex rings. *J. Fluid Mech.* **230**, 583–646.

Lee, S., Lele, S. K. & Moin, P. 1993 Direct numerical simulation of isotropic turbulence interacting with a weak shock wave. *J. Fluid Mech.* **251**, 533–562.

Lilly, D. K. 1992 A proposed modification of the Germano subgrid-scale closure method. *Phys. Fluids* A **4**, 633–635.

Lim, J., Choi, H. & Kim, J. 1998 Control of streamwise vortices with uniform magnetic fluxes. *Phys. Fluids* **10**, 1997–2005.

Löhner, R. & Yang, C. 2002 Vorticity confinement on unstructured grids. *AIAA Paper* 2002–0137.

Löhner, R., Yang, C. & Roger, R. 2002 Tracking vortices over large distances using

vorticity confinement. *Proc. Twenty-Fourth Symposium on Naval Hydrodynamics*, Fukuoka, Japan, July 8–13.

Moulton, M. & Steinhoff, J. 2000 A technique for the simulation of stall with coarse-grid CFD. *AIAA Paper* 2000–0277.

Murayama, M., Nakahashi, K. & Obayashi, S. 2001 Numerical simulation of vortical flows using vorticity confinement coupled with unstructured grid. *AIAA Paper* 2001–0606.

Orlandi, P. 1990 Vortex dipole rebound from a wall. *Phys. Fluids* A **2**, 1429–1436.

Robinson, M. A. 2004 Application of vorticity confinement to inviscid missile force and moment prediction. *AIAA Paper* 2004–0717.

Roe, P. 2001 Vorticity capturing. *AIAA Paper* 2001–2523.

Steinhoff, J. & Lynn, N. 2004 Treatment of vortical flow using vorticity confinement. UTSI Preprint, University of Tennessee Space Institute, Tullahoma, Tenn., November.

Steinhoff, J., Lynn, N. & Wang, L. 2005 Computation of high Reynolds number flows using vorticity confinement: I. Formulation. UTSI Preprint, University of Tennessee Space Institute, Tullahoma, Tenn., March.

Steinhoff, J. & Underhill, D. 1994 Modification of the Euler equations for "vorticity confinement": Application to the computation of interacting vortex rings. *Phys. Fluids* A **6**, 2738–2744.

Steinhoff, J., Yonghu, W., Mersch, T. & Senge, H. 1992 Computational vorticity capturing: Application to helicopter rotor flow. *AIAA Paper* 1992–0056.

Strawn, R. 2000 Computational modeling of hovering rotors and wakes. *AIAA Paper* 2000–0110.

Wang, C. M., Steinhoff, J. S. & Wenren, Y. 1995 Numerical vorticity confinement for vortex–solid body interaction problems.*AIAA J.* **33**, 1447–1453.

Wenren, Y., Walter, J., Fan, M. & Steinhoff, J. 2006 Vorticity confinement and advanced rendering to compute and visualize complex flows *AIAA Paper* 2006–0945.

Zang, T. A. 1991 On the rotation and skew-symmetric forms for incompressible flow simulations. *Appl. Numer. Math.* **7**, 27–40.